CHEMBIOCHEM

DOI: 10.1002/cbic.200800119

# Catalyzed Oxidative Corrosion of Porous Silicon Used as an Optical Transducer for Ligand–Receptor Interactions

Nicolas H. Voelcker,*[a] Ignacio Alfonso,[b] and M. Reza Ghadiri*[c]

*Biosensors fabricated on the nanoscale offer exciting new avenues in the quest for better understanding and characterization of biological systems. Porous silicon is an ideal nanostructured material for the construction of optical transducer matrices because it is easily functionalized with biomolecular probes and displays strong optical interferences. Here, we show that certain transition metal complexes, including nickel(II)cyclam, are able to induce corrosion in porous silicon films rapidly, generating a strong optical interferometric signal that originates from the porous layer. We subsequently exploit this effect to design a transducer for ligand–receptor recognition. With a nickel(II)cyclam derivative as a catalytic label, DNA- and avidin-binding events are detected by time-lapse interferometric reflectance spectroscopy in a fast, simple, and inexpensive fashion.*

## Introduction

Significant efforts are currently being devoted to the development of biosensors that exploit signal amplification to boost sensitivity.[1–6] These studies are fueled by the need for rapid and sensitive sensors in areas such as biomedical diagnostics and veterinary, food, and environmental monitoring, as well as bioterrorism prevention. Signal amplifying elements are commonly incorporated into biosensors through activation of an enzymatic pathway[1,7–9] by use of appropriate processes based on organic or organometallic reactions or on the catalytic properties of metallic nanoparticles.[10–13]

However, the involvement of a non-metallic inorganic material in the critical signal amplification step has been rare. Porous silicon is a nanostructured material with a large surface area and unique electrical[14] and optical properties[15] that have been exploited by several groups for the development of biosensor devices.[16–24] As one example, the photoluminescence of porous silicon is altered upon incorporation of molecules in the porous layer.[17,25,26]

Another common strategy is the fabrication of interferometric sensors[27–31] in which molecular recognition events can be monitored by a red shift in the Fabry–Perot fringe pattern that is essentially caused by a change in the refractive index of the porous layer upon analyte binding.[19,32] By interferometric reflectance spectroscopy, biomolecules such as streptavidin, immunoglobulins, and DNA have been detected in low concentrations.[30,33–35] However, these sensors are generally characterized by linear signal–response curves and often cannot incorporate signal amplifying elements, ultimately limiting their achievable sensitivity.

We have previously established a unique mechanism for DNA detection using an interferometric biosensor based on *p*-type porous silicon.[16,36] Our method relies on the hybridization of a negatively charged DNA target to its complementary strand immobilized on the silicon surface, which induces the corrosion (oxidation–hydrolysis) of the porous interference layer. While reflectance spectroscopy is typically not useful for the detection of low concentrations of DNA-like molecules, the binding-induced corrosion effectively amplifies the spectroscopic signal through the profound morphological change in the solid support, an effect akin to the amplification of the binding event in an enzyme-linked immunoassay.[37] As our previous sensors were limited to DNA detection, we set out here to find a more general biosensor design framework that exploits the accelerated corrosion of a porous silicon substrate to amplify the analyte binding signal. We hypothesized that a suitable chemical catalyst of porous silicon corrosion could be localized at the surface of the silicon matrix by tethering it to a ligand for a surface-immobilized receptor (Scheme 1). The specific ligand–receptor interaction would thus afford a high effective concentration of the corrosion catalyst in the porous layer, accelerating oxidation and corrosion of the porous silicon matrix, and thereby amplifying the signal of the ligand-binding event.

Transition metal complexes derived from polyazamacrocycles and salen-type ligands are a growing class of catalysts with expanding utility in a variety of chemical transformations.[38–42] These complexes also show promise as biomimetic

[a] *Prof. Dr. N. H. Voelcker*
*School of Chemistry, Physics and Earth Sciences, Flinders University*
*Adelaide, SA 5001 (Australia)*
*Fax: (+61) 8-8201-2905*
*E-mail: nico.voelcker@flinders.edu.au*

[b] *Dr. I. Alfonso*
*Department of Biological Organic Chemistry*
*Chemical and Environmental Research Institute (IIQAB)*
*Spanish Council for Scientific Research (CSIC)*
*08034 Barcelona (Spain)*

[c] *Prof. Dr. M. R. Ghadiri*
*Departments of Chemistry and Molecular Biology*
*The Skaggs Institute for Chemical Biology*
*The Scripps Research Institute*
*La Jolla, CA 92037 (USA)*
*Fax: (+1) 858-784-2798*
*E-mail: ghadiri@scripps.edu*

  

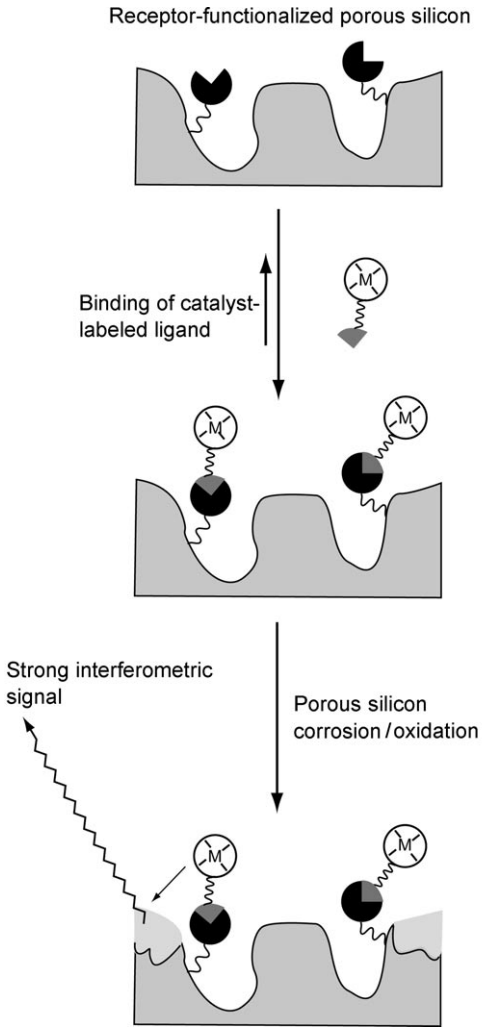


**Scheme 1.** Transducer design based on the catalysis of oxidative corrosion of a porous silicon matrix.

catalysts for the hydrolytic cleavage of peptide bonds[43,44] and for the induction of oxidative damage or cleavage of DNA.[45–47] We conjectured that such transition metal complexes might also be capable of inducing oxidative hydrolysis of a porous silicon matrix.

Accordingly, we prepared a number of salen and cyclam complexes that were known to possess oxidative or hydrolytic activities and studied their effectiveness in catalyzing porous silicon corrosion. Interferometric reflectance spectroscopy (IRS) and atomic force microscopy (AFM) were used to characterize the optical and morphological changes, respectively, in the porous silicon layer. Building on findings from these initial studies, we fashioned an optical transducer of DNA–DNA and avidin–biotin interactions, in which biomolecule binding is transduced into an optical response of the porous silicon layer. This transducer shows potential for use in optical biosensors, which—although being single-use—would nevertheless be attractive for applications in point-of-care or laboratory diagnostics, or in workplace or roadside testing. In these cases, simple, fast, and miniaturizable transduction platforms are required, and single-use devices are preferred over reusable ones.

## Results and Discussion

### Preparation of porous silicon interference layers

Macroporous silicon was fabricated by anodizing heavily doped *p*-type ($p^{++}$) silicon wafers in ethanolic HF solution. Pores larger than 50 nm are desirable in order to minimize steric hindrance for the entry of large analytes such as DNA or proteins into the porous layer. We adjusted the etching conditions to obtain pores of 100 to 300 nm diameter as measured by AFM.[30] The predominantly silicon-hydride-terminated porous silicon surface was subsequently oxidized with ozone. Time-lapse IRS confirmed that the porous layers prepared in this fashion were sufficiently stable towards hydrolysis in neutral aqueous medium. When the effective optical thickness (EOT) of the porous silicon layer was plotted against incubation time, a decrease in EOT of 15–17 nm min$^{-1}$ was measured for the freshly etched porous silicon. This EOT drift is due to the conversion of silicon into silica, leading to a decrease in the effective refractive index ($n_{eff}$) of the porous silicon layer. Furthermore, dissolution of the porous layer results in a decrease in the layer thickness ($l$) or an increase in porosity. Given that $EOT = l n_{eff}$, both oxidation and dissolution lead to a decay in EOT.[36] Ozone oxidation is known to stabilize the porous silicon against rapid oxidation and corrosion,[30,36] and in accordance with this stabilizing effect, smaller EOT decays of about 0.2–0.4 nm min$^{-1}$ were measured.

### Porous silicon corrosion catalyzed by transition metal complexes

Cyclam- and salen-based transition metal complexes have been used as catalysts in a variety of chemical reactions including epoxidations and hydroxylations.[38–42] Several groups have demonstrated the use of these complexes as potent enzyme mimics in a variety of biomolecule fragmentation and oxidation reactions.[44,48–51] Inspired by these studies, we investigated several bis(salicylidene)ethylenediamine (salen) and 1,4,8,11-tetraazacyclotetradecane (cyclam) complexes of $Cu^{II}$, $Zn^{II}$, $Ti^{IV}$, $Cr^{III}$, $Mn^{III}$, $Fe^{II}$, $Ru^{III}$, $Co^{II}$, $Rh^{III}$, and $Ni^{II}$ for their activity in corroding porous silicon layers. As well as the commercially available parent salen ligand, bishydroxysalen was also synthesized. This ligand was thought to create a hydroquinone system cooperating with the transition metal redox system in the complex, leading to higher efficiency in DNA cleavage. Changes to the Fabry–Perot fringe pattern of ozone-oxidized porous silicon upon incubation in millimolar solutions of metal complexes were recorded by time-lapse IRS. Oxidant (ammonium persulfate) or reductant (dithiothreitol) was added in some cases to increase oxidative or hydrolytic potency. The obtained normalized EOT slope changes are listed in Table 1.

The results of a screening of transition metal complexes revealed that the cyclam macrocyclic complexes of $Ni^{II}$ and $Cu^{II}$ in the presence of ammonium persulfate, as well as the bishydroxysalen complexes of $Cu^{II}$, $Ru^{III}$ and $Fe^{II}$, induced rapid porous silicon corrosion (Table 1). The highest EOT change—$(\Delta EOT/\Delta t)/EOT_0$—was observed for $Ni^{II}$cyclam in the presence

  

of oxidant. Figure 1 shows the measured EOT traces for porous silicon in contact with $Ni^{II}$cyclam and $Ru^{III}$bishydroxysalen solutions. The background EOT slope for this experiment was about $-0.2\,nm\,min^{-1}$. Upon addition of nickel cyclam in the presence of $(NH_4)_2S_2O_8$ the EOT slope increased to $-6.1\,nm\,min^{-1}$, whereas addition of $Ru^{III}$bishydroxysalen gave a slope of $-1.93\,nm\,min^{-1}$. These are equivalent to 30- or tenfold increases, respectively, in the corrosion rates. Control reactions in which porous silicon was exposed to millimolar solutions of the metal salts, the ligands, the oxidant, or the reductant alone did not affect the background rate of porous silicon corrosion. We verified by AFM imaging that the changes in the EOT slope were due to pore widening and collapse (data not shown). From these measurements, we concluded that $Ni^{II}$cyclam was the most effective catalyst, and further studies therefore utilized this particular complex.

**Table 1.** Observed change in effective optical thickness (EOT) of porous silicon substrates under various conditions.

| Complex | $-(\Delta EOT/\Delta t)/EOT_0\times10^3$ [$min^{-1}$] Background | Complex | + oxidant | + reductant |
|---|---|---|---|---|
| $Cu^{II}$salen | 0.034 | 0.028 | – | 0.038 |
| $Cu^{II}$bishydroxysalen | 0.039 | 0.232 | – | 0.195 |
| $Cu^{II}$phenylensalen | 0.035 | 0.039 | – | 0.032 |
| $Cu^{II}$cyclam | 0.103 | 0.228 | 0.386 | 0.112 |
| $Ni^{II}$salen | 0.026 | 0.036 | 0.040 | – |
| $Ni^{II}$bishydroxysalen | 0.029 | 0.068 | | – |
| $Ni^{II}$cyclam | 0.053 | 0.084 | **1.161** | – |
| $Zn^{II}$salen | 0.023 | 0.064 | 0.084 | – |
| $Zn^{II}$cyclam | 0.062 | 0.040 | 0.021 | – |
| $Fe^{II}$bishydroxysalen | 0.085 | 0.329 | 0.216 | 0.211 |
| $Fe^{II}$cyclam | 0.048 | 0.152 | 0.101 | – |
| $Co^{II}$salen | 0.038 | 0.039 | 0.038 | 0.163 |
| $Co^{II}$cyclam | 0.056 | 0.134 | 0.166 | 0.199 |
| $Mn^{III}$salen | 0.024 | 0.035 | 0.028 | – |
| $Mn^{III}$cyclam | 0.019 | 0.039 | 0.042 | – |
| $Ti^{IV}$salen | 0.052 | 0.058 | | – |
| $Ti^{IV}$cyclam | 0.116 | 0.052 | 0.015 | 0.107 |
| $Ru^{III}$bishydroxysalen | 0.085 | 0.374 | 0.374 | |
| $Ru^{III}$cyclam | 0.091 | 0.143 | 0.340 | – |
| $Cr^{III}$salen | 0.073 | 0.092 | 0.126 | – |
| $Cr^{III}$cyclam | 0.057 | 0.073 | 0.083 | – |
| $Rh^{III}$salen | 0.084 | 0.156 | 0.178 | – |
| $Rh^{III}$cyclam | 0.104 | 0.113 | 0.134 | – |

[a] Data were obtained from time-lapse interferometric reflectance spectroscopy (IRS) measurements on porous silicon films etched at 250 $mA\,cm^{-2}$ upon incubation with solutions of metal complexes (1 mM) in PBS (100 mM, pH 7.0). Incubation times of at least 20 min were allowed for each measurement. Ammonium persulfate or DTT (1 mM) were used as oxidant or reductant, respectively. The EOT slope ($\Delta EOT/\Delta t$) was calculated and divided by the initial EOT ($EOT_0$).

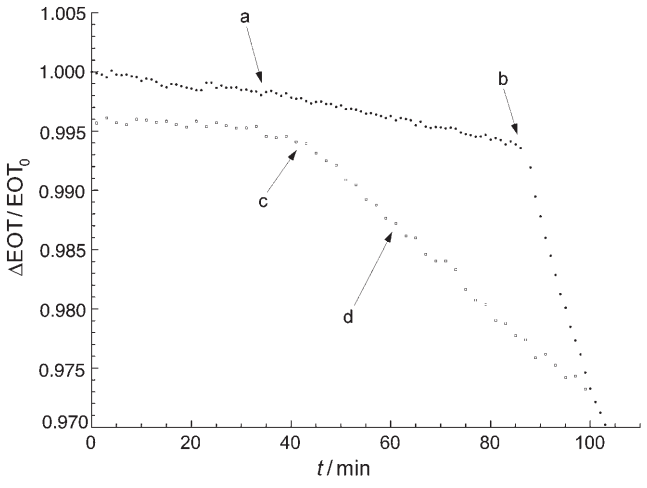


**Figure 1.** Change in effective optical thickness ($\Delta EOT/EOT_0$) over time for an ozone-oxidized porous silicon chip etched at 250 $mA\,cm^{-2}$. The measurement was carried out in phosphate buffer (100 mM) at pH 7.0. Two different experiments are shown: (○) a) Addition of $Ni^{II}$cyclam (1 mM); b) addition of $Ni^{II}$cyclam (1 mM) in the presence of $(NH_4)_2S_2O_8$ (1 mM); (■) c) addition of $Ru^{III}$bishydroxysalen (1 mM); and d) addition of $Ru^{III}$bishydroxysalen (1 mM) in the presence of $(NH_4)_2S_2O_8$ (1 mM).

### Redox behavior of $Ni^{II}$cyclam

Several oxidizing agents convert $Ni^{II}$cyclam into a radical $Ni^{III}$ species;[52–55] we carried out experiments to study the $Ni^{II}$cyclam in the presence of ammonium persulfate. The parent complex shows a characteristic UV absorption with a maximum at 456 nm and an extinction coefficient of $52\,M^{-1}\,cm^{-1}$. Upon addition of oxidant, we observed the disappearance of the absorption band at 456 nm and the emergence of a new absorption band peaking at 353 nm ($\varepsilon = 1289\,M^{-1}\,cm^{-1}$), consistent with the formation of $Ni^{III}$cyclam. The $^1H$ NMR spectrum of $Ni^{II}$cyclam was of low signal intensity, as would be expected for a compound existing in equilibrium between its paramagnetic high-spin and diamagnetic low-spin forms. Upon addition of oxidant, we observed the complete disappearance of NMR signals, which can be explained by increased paramagnetism in the sample, again consistent with the formation of a $Ni^{III}$ species.

Finally, the oxidation of $Ni^{II}$ to $Ni^{III}$ was also monitored by ESI mass spectrometry. Upon addition of oxidant, the peak at *m/z* 257 ($[Ni^{II}cyclam-H]^+$) disappeared and gave rise to a peak at *m/z* 256 ($[Ni^{III}cyclam-2H]^+$). After 7 days, mass spectra were again acquired. Whilst an aged $Ni^{II}$cyclam sample could not be distinguished mass spectrometrically from a freshly prepared complex, the aged oxidized $Ni^{II}$cyclam showed a weak peak at *m/z* 256 and two additional strong peaks at *m/z* 255 and 257. This can be interpreted in terms of a disproportionation of $Ni^{III}$ to $Ni^{IV}$ and $Ni^{II}$ or alternatively in terms of the formation of an unsaturated ligand species. These results are also consistent with UV monitoring experiments of the oxidized $Ni^{II}$cyclam at 353 nm, which showed a $6\,\%\,h^{-1}$ absorbance decrease. Interestingly, the NMR results indicate that some $Ni^{III}$ still remained after seven days. These results indicate that $Ni^{III}$cyclam is the reactive species in contact with porous silicon.

We next carried out a series of investigations to unravel the mechanism of porous silicon corrosion by this metal complex. To elucidate whether the process is a radical oxidation or a hydrolytic reaction, we performed the following quenching experiments. The addition of *p*-hydroquinone solution (10 mM) to a mixture containing the $Ni^{II}$cyclam and ammonium persulfate (both 1 mM) completely inhibited the silicon degradation, a result suggestive of a radical oxidation mechanism. On the

  

other hand, the presence of EtOH or *t*BuOH (100 mM) failed to inhibit corrosion of the surface. This result indicates that a caged or partially ligated sulfate radical species is formed, as has also been proposed for other nickel-complex-catalyzed oxidations.[56] Concluding these results, we confirmed that the active species involved in porous silicon degradation is the $Ni^{III}$cyclam-sulfate radical and that this species is stable enough to be useful in 2–3 h assays.

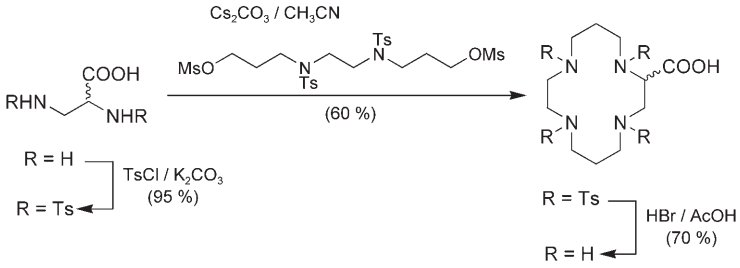


**Scheme 2.** Preparation of a carboxy-derivatized cyclam ligand.

### Preparation of a modified cyclam ligand

The parent cyclam ligand does not contain a reactive functional group suitable for conjugation to biomolecules, so derivatization with an anchoring moiety was necessary. We anticipated that substitution on a nitrogen might change the interaction between the metal and ligand, possibly compromising the catalytic properties of the $Ni^{II}$ cyclam complex. We hence synthesized a modified cyclam ligand with a *C*-pendant carboxy group, using a modification of the Richman–Atkins procedure of cesium carbonate-promoted coupling between a carboxyethylene-bis(sulfonamide) and the corresponding bis-electrophilic system to construct the cyclic structure.[57] Subsequent hydrolysis yielded the *C*-carboxy-derivatized cyclam (Scheme 2). The $Ni^{II}$cyclam complex was formed in DMF at elevated temperature. Complex formation was followed by monitoring the UV absorption of the complex at 450 nm.

Ozone-oxidized porous silicon was incubated with the derivatized $Ni^{II}$cyclam (1 mM), and the EOT slope was recorded by time-lapse IRS. The EOT background slope was $-0.31\ nm\,min^{-1}$ for PBS (100 mM) alone and $-0.40\ nm\,min^{-1}$ for derivatized $Ni^{II}$cyclam without oxidant. Upon addition of ammonium persulfate (1 mM), the negative slope increased in magnitude to $-3.64\ nm\,min^{-1}$. The carboxy-derivatized analogue of the $Ni^{II}$cyclam was thus confirmed to be an efficient catalyst for the corrosion of porous silicon.

### Labeling biomolecules with $Ni^{II}$cyclam

The carboxy-functionalized $Ni^{II}$cyclam derivative was next conjugated to DNA and biotin as shown in Scheme 3.

We anticipated that conjugating the pre-formed $Ni^{II}$cyclam complex to DNA would prevent chelation or electrostatic sequestration of free nickel ions by the oligonucleotide.[58] Such ionic interactions could interfere with DNA hybridization, since $Ni^{II}$ binding is known to destabilize the B-DNA double helix.[59]

We therefore investigated the effects of $Ni^{II}$cyclam attachment to DNA oligonucleotides both on hybridization properties and on stability. DNA melting curves in the presence of $Ni^{II}$cyclam or $Ni^{II}$cyclam attached to DNA did not differ from curves obtained in the absence of the complex. However, upon addition of oxidant, the absorption of nucleobases at

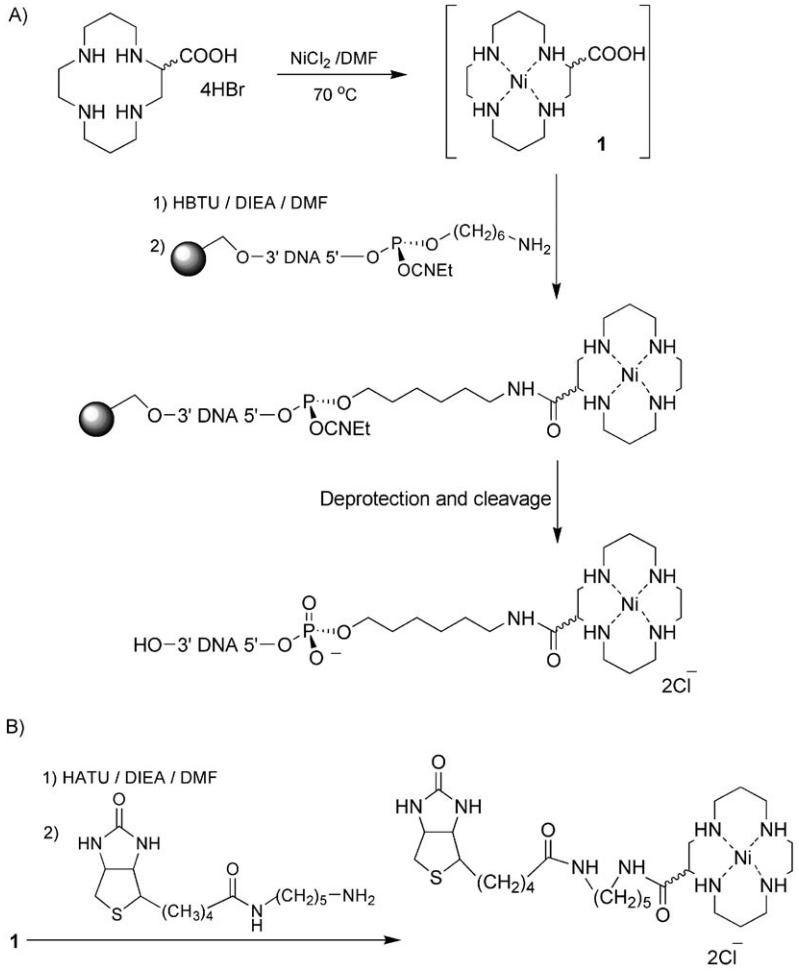


**Scheme 3.** Conjugation of the derivatized $Ni^{II}$cyclam to A) DNA, and B) biotin.

  

260 nm above 60 °C decreased irreversibly, suggesting DNA damage (data not shown). Notably, no significant change in optical density at 260 nm was observed for $Ni^{II}$cyclam-DNA (2 μM) in the presence of ammonium persulfate (1 mM) at room temperature over 24 h ($< 0.1\%\,h^{-}$). The amount of DNA strand cleavage induced by $Ni^{II}$cyclam plus oxidant was assessed by electrophoresis in a denaturing acrylamide gel. Strand cleavage was absent over 24 h at room temperature (data not shown).

These results show that the $Ni^{II}$cyclam DNA conjugate is sufficiently stable for hybridization experiments at room temperature even in the presence of oxidant.

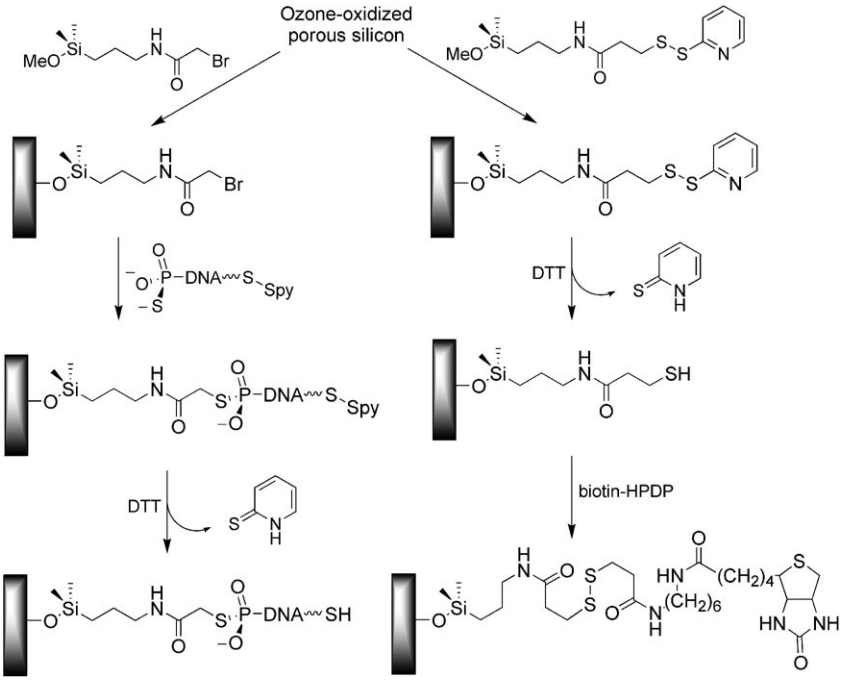


**Scheme 4.** Functionalization of ozone-oxidized porous silicon.

### Surface modification of porous silicon interference layers

Porous silicon was functionalized to allow the immobilization of receptors in the porous layer. Characterization of surface chemistry was carried out by diffuse reflectance FTIR. Spectra of freshly etched silicon wafers show the characteristic bands at 2110 and 2090 $cm^{-1}$ ($\nu_{Si-H_2}$and $\nu_{H-SiO}$). The most prominent feature in IR spectra of $p^{++}$ porous silicon is the broad interference band peaking at 1950 $cm^{-1}$.[15,60] Ozone oxidation leads to disappearance of the Si–H vibrational band and the appearance of a strong band at 1052 $cm^{-1}$ ($\nu_{Si-O-Si}$). Silanizations on the oxidized porous silicon surface were subsequently carried out as shown in Scheme 4.

Upon functionalization with [3-(2-bromoacetamido)propyl]dimethylmethoxysilane, the surface displays additional bands attributable to the linker (Figure 2A): a band at 3290 $cm^{-1}$ (amide A), the amide I band at 1662 $cm^{-1}$, and the amide II band at 1549 $cm^{-1}$. The aliphatic stretching vibrational bands are also visible (at 2953, 2929, and 2860 $cm^{-1}$; Figure 2A, inset). Functionalization with (2-pyridyldithiopropionamidopropyl)dimethylmethoxysilane leads to a surface that displays the above bands (amide A at 3290 $cm^{-1}$, the amide I band at 1651 $cm^{-1}$, and the amide II band at 1567 $cm^{-1}$) and in addition an aromatic C–H stretching vibration at 3079 $cm^{-1}$ (Figure 2B, inset).

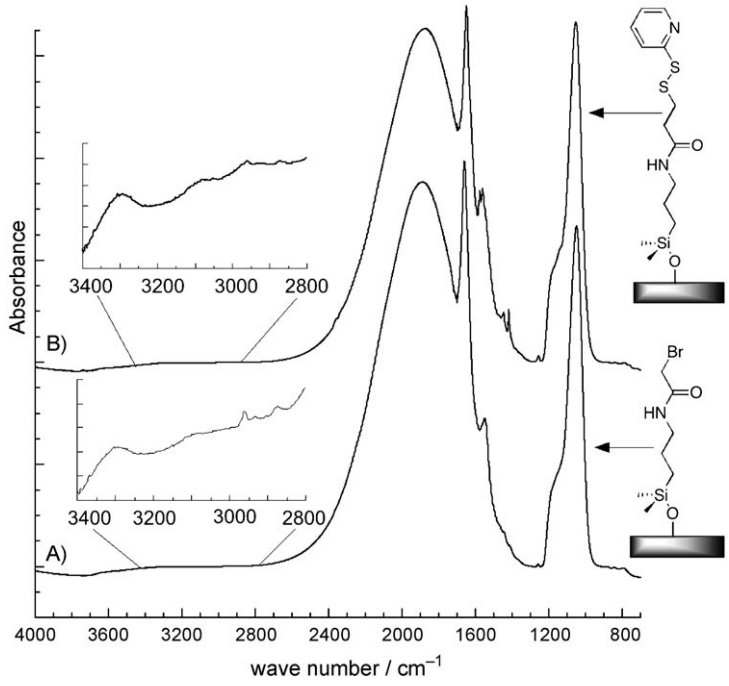


**Figure 2.** FTIR spectra of ozone-oxidized porous silicon layers derivatized with A) [3-(2-bromoacetamido)propyl]dimethylmonomethoxysilane and B) (2 pyridyldithiopropionamidopropyl)-dimethylmonomethoxysilane. The broad band with a maximum at 1950 $cm^{-1}$ is attributed to an IR interference effect.

In order to quantify the surface coverage of the silane linker, the disulfide was reduced with dithiothreitol (DTT) to release pyridine-2-thione (Scheme 4). This reporter molecule could be detected by UV/Vis spectroscopy ($\lambda_{max} = 343$ nm, $\varepsilon = 8080\,M^{-1}\,cm^{-1}$). Using the pyridine-2-thione reporter, we calculated the number of reactive functional groups to be 10–30 $nmol\,cm^{-2}$.

  

A 5′-thiophosphate-modified oligonucleotide was immobilized by alkylation of the [3-(2-bromoacetamido)propyl]dimethylmethoxysilane-modified surface (Scheme 4, left). The amount of immobilized DNA was determined by reading the UV absorption of the supernatant at 260 nm before and after immobilization. We also immobilized 5′-thiophosphate-3′-pyridyldisulfide DNA and quantified the amount of pyridine-2-thione released by DTT. The DNA coverages obtained from both methods are in good agreement (1–2 nmol $cm^{-2}$). Finally, experiments employing 3′-fluorescein-5′-thiophosphate DNA showed a decrease in solution fluorescence over 2–3 h that allowed us to calculate a similar surface coverage of 2–3 nmol $cm^{-2}$. This number is at least one order of magnitude higher than that of a monolayer on a flat surface. However, this surface coverage is still low in relation to the actual available surface area of a porous silicon chip.

Biotin was also immobilized on the thiol-functional porous silicon surface (Scheme 4, right). The reaction of *N*-[6-(biotinamido)hexyl]-3-(2-pyridyldithio)propionamide (biotin–HPDP) on a thiol-functional porous silicon surface proceeded smoothly by disulfide exchange and afforded a surface coverage of 5–10 nmol biotin per $cm^2$ (determined by UV monitoring of released pyridine-2-thione). The amount of probe molecules immobilized on the porous silicon far exceeds the theoretical monolayer coverage of a flat film. We calculated that approximately 8–16% of the actual pore surface is covered with biotin.[30]

It should be noted that functionalization of the porous silicon surface further stabilized the surface in aqueous medium by capping of oxidation-susceptible sites and suppressing oxidation and dissolution processes. The EOT decays for functionalized porous silicon are of the order of 0.03–0.08 nm $min^{-1}$.

Upon addition of a 1 mM solution of $Ni^{II}$cyclam in the presence of oxidant, the EOT slope changes to $-0.75$ nm $min^{-1}$. This is equivalent to a 15-fold increase in slope steepness and we conclude that even silanized porous silicon is still susceptible to $Ni^{II}$cyclam induced pore corrosion.

### Interferometric detection of DNA hybridization

We undertook the following studies to investigate whether $Ni^{II}$cyclam-labeled biomolecules could transduce specific bimolecular recognition into an optical response of the surface. Our first focus was on the detection of DNA hybridization (Figure 3). The porous silicon surface was first functionalized with the 16-mer DNA1 (attached through the 5′ terminus) and then exposed to a solution (~1 μM) of noncomplementary DNA2–$Ni^{II}$cyclam (point a, Figure 3A). The EOT slope was not affected either in the absence (point a) or in the presence of ammonium persulfate (point b). After a buffer wash cycle (point c), the functionalized porous silicon was exposed to a solution (~1 μM) of the complementary DNA1–$Ni^{II}$cyclam (labeled with $Ni^{II}$cyclam on the 5′ terminus; point d). Again, no appreciable change in the EOT was detected. Similarly, addition of complementary DNA without $Ni^{II}$cyclam label did not result in EOT slope changes. Successful hybridization of DNA in the pores was confirmed by experiments with fluorescently labeled

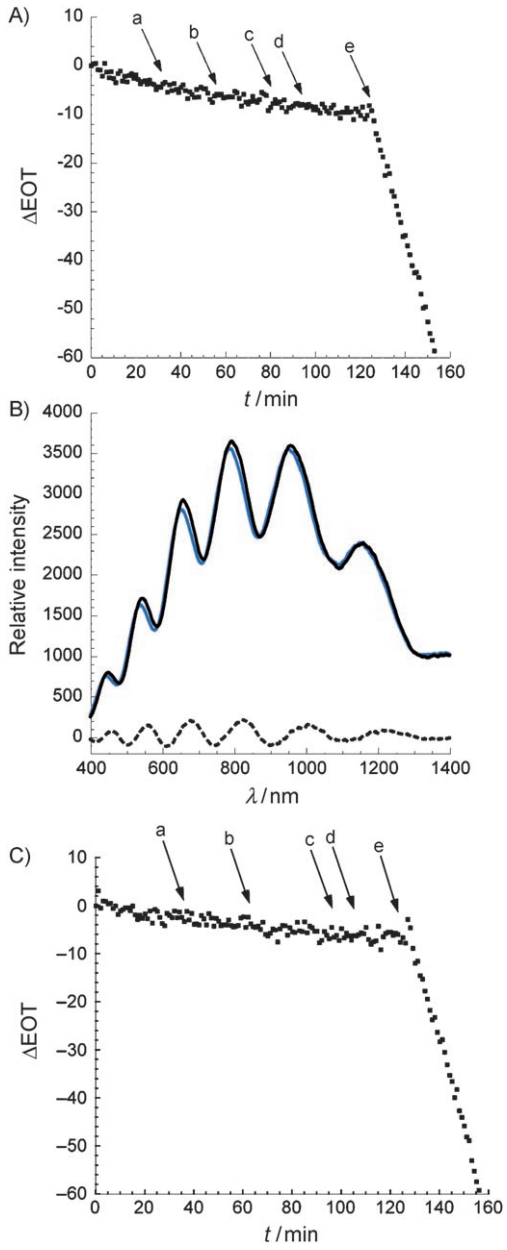


**Figure 3.** A) Change in effective optical thickness (ΔEOT) of porous silicon derivatized with 5′-thiophosphate DNA1 over time. a) Addition of noncomplementary 5′-$Ni^{II}$cyclam DNA (DNA2) (1 μM); b) addition of $(NH_4)_2S_2O_8$ (1 mM); c) washing with buffer; d) addition of complementary 5′-$Ni^{II}$cyclam DNA (DNA1) (1 μM); e) addition of $(NH_4)_2S_2O_8$ (1 mM). The measurement was carried out on a $p^{++}$ porous silicon layer in phosphate buffer (100 mM, pH 7.0) functionalized with [3-(2-bromoacetamido)propyl]dimethylmonomethoxysilane and 5′-thiophosphate DNA1. B) Interferometric reflectance spectra of biotin-functionalized porous silicon. (——) Before exposure to complementary DNA; (——) after 20 min incubation with complementary 5′-$Ni^{II}$cyclam DNA (DNA1) (1 μM) and $(NH_4)_2S_2O_8$ (1 mM); and (-----) difference spectra (difference between black and blue trace). C) Change in effective optical thickness (ΔEOT) of a porous silicon chip derivatized with 3′-thiophosphate DNA1 over time. a) Addition of noncomplementary 5′-$Ni^{II}$cyclam DNA (DNA2) (1 μM); b) addition of $(NH_4)_2S_2O_8$ (1 mM); c) washing with buffer; d) addition of complementary 5′-$Ni^{II}$cyclam DNA (DNA1) (1 μM); e) addition of $(NH_4)_2S_2O_8$ (1 mM). This measurement was carried out on a $p^{++}$ porous silicon layer in phosphate buffer (100 mM, pH 7.0) functionalized with [3-(2-bromoacetamido)propyl]dimethylmonomethoxysilane and 3′-thiophosphate DNA1.

  

DNA (data not shown). These results show that mere hybridization of DNA in the pores does not lead to measurable interferometric reflectance changes.

However, upon addition of a solution (1 μM) of $(NH_4)_2S_2O_8$ (point e) activating the catalyst, the EOT slope decreased by a factor of 24, from $-0.07$ nm min$^{-1}$ (background corrosion) to $-1.70$ nm min$^{-1}$, consistently with the onset of a rapid pore corrosion, suggesting an amplification of the original binding signal. The net change in EOT upon DNA1–Ni$^{II}$cyclam recognition before and after exposure to complementary DNA is about 8 nm. The symmetric line shape of the difference reflectance spectrum in Figure 3B (dashed line) is indicative of wavelength shifting of the interference fringe pattern after exposure to complementary DNA.

Conversely, under similar experimental conditions, porous silicon functionalized with DNA2 displayed a significant change in the slope of EOT when exposed to the complementary DNA2–Ni$^{II}$cyclam, but not in the presence of noncomplementary DNA1--Ni$^{II}$cyclam.

We also performed a binding experiment with a porous silicon chip functionalized with 3′-thiophosphate DNA1 (Figure 3C). In this scenario, the complex conjugated to the 5′ end of DNA1 ultimately comes close to the porous silicon surface upon hybridization to DNA1. With 3′-thiophosphate DNA1 functionalized porous silicon and DNA1–Ni$^{II}$cyclam (labeled with Ni$^{II}$cyclam on the 5′-terminus), the slope steepness increased 30-fold (from $-0.06$ nm min$^{-1}$ to $-1.8$ nm min$^{-1}$). The somewhat better optical response in relation to the experiment shown in Figure 3A might be explained by the fact that the Ni$^{II}$cyclam complex resides in closer proximity to the surface.

In order to verify that the EOT slope changes were indeed due to pore oxidation and collapse, the chip surface was examined by AFM (Figure 4). The ozone-oxidized $p^{++}$ chip etched at 250 mA cm$^{-2}$ had pore radii of 80–200 nm (Figure 4A). The chip was then functionalized with [3-(2-bromoacetamido)propyl]dimethylmethoxysilane and with DNA1. These reactions did not affect the morphology of the porous layer on this image scale (2 μm). However, when the porous silicon surface was imaged after 90 min incubation with a solution of the complementary DNA strand (DNA1–Ni$^{II}$cyclam, 1 μM), channel-like structures appeared and the pore size increased significantly (300–500 nm, Figure 4B). The observed channels can be interpreted in terms of fused pores due to pore wall collapse. We believe that the corrosion is initiated at patches on the porous silicon surface with incomplete linker coverage.

### Interferometric detection of biotin–avidin binding

We postulated that the strategy used above for DNA detection would also be applicable to the detection of proteins. To confirm this possibility, we chose the well known high-affinity interaction between biotin and avidin. A biotinylated porous silicon chip was exposed to a solution of avidin (1 μM, Figure 5A, point a). The observed increase in the EOT slope can be interpreted in terms of the higher refractive index of proteins relative to water. Clearly, this effect was not due to the bulk effect of the protein solution, because subsequent washing of the surface with PBS buffer did not reduce the EOT (point b). Neither did the addition of oxidant (1 mM) to the avidin modified surface affect the EOT slope (point c). After a washing step (point d), a solution of Ni$^{II}$cyclam-conjugated biotin (100 μM) was added (point e). Binding of the biotin–metal complex conjugate to surface-anchored avidin did not result in significant changes in the EOT slope. We again washed the surface with buffer in order to remove any unspecifically bound biotin–Ni$^{II}$cyclam conjugate (point f). A dramatic change in the EOT slope could be induced by activating the catalyst upon addition of a millimolar solution of $(NH_4)_2S_2O_8$ (point g). The EOT slope decreased by a factor of 48 ($-0.03$ nm min$^{-1}$ to $-1.45$ nm min$^{-1}$) relative to background corrosion. Figure 5B shows the Fabry–Perot fringes before the experiment, after 20 min exposure to avidin (red shift), and after incubation with biotin–Ni$^{II}$cyclam and oxidant (blue shift). As expected, specific binding of avidin to the biotinylated porous layer leads to a red shift in the fringe pattern, due to a net refractive index increase upon infiltration of the porous layer. After a 20 min incubation with the Ni$^{II}$cyclam-labeled biotin and oxidant, we observed a significant blue shift relative to the fringe pattern acquired immediately before the experiment.

As in the case of DNA binding, AFM images of the avidin sensor showed porous silicon corrosion upon biotin–Ni$^{II}$cyclam binding. Initially, the surface of the biotinylated sensor chip imaged by AFM showed a morphology virtually identical to that seen in the AFM image in Figure 4A. However, after incubation first with avidin, and then with biotin–Ni$^{II}$cyclam and ox-

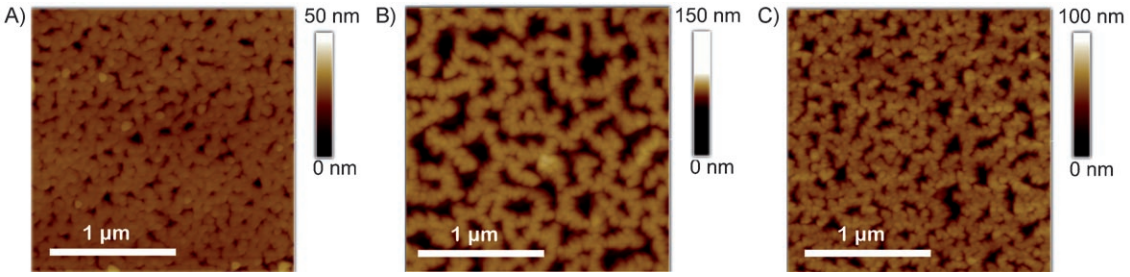


**Figure 4.** Tapping mode AFM images of porous silicon. A) AFM image of ozone-oxidized porous silicon, B) AFM image of porous silicon derivatized with [3-(2-bromoacetamido)propyl]dimethylmonomethoxysilane and 3′-thiophosphate DNA1 after 1 h incubation with Ni$^{II}$cyclam-DNA1 (1 μM) and oxidant (1 mM), and C) AFM of biotin-functionalized porous silicon layer after 90 min incubation with avidin (1 μM), biotin–Ni$^{II}$cyclam (100 μM), and oxidant (1 mM). Lateral scale is $2\times2$ μm$^2$.

  

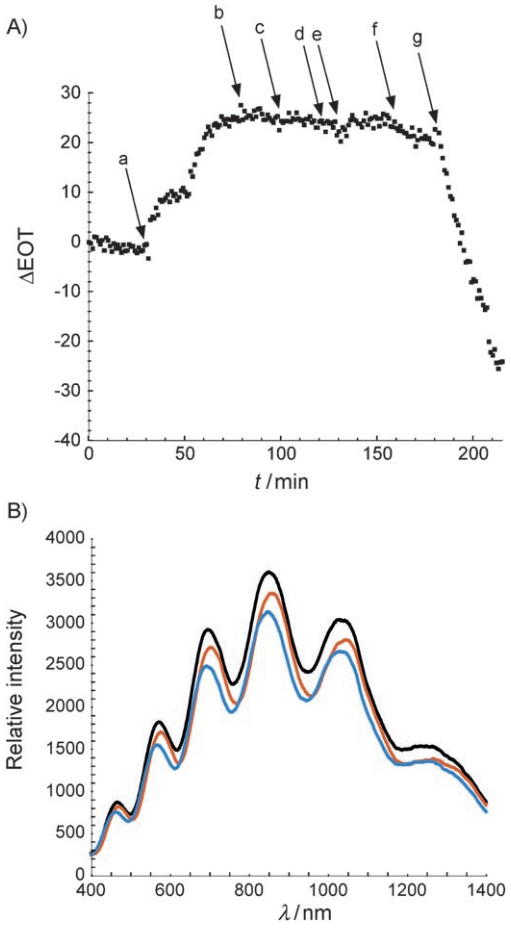


**Figure 5.** A) Change in effective optical thickness (ΔEOT) over time of a biotin-functionalized porous silicon chip in phosphate (100 mM, pH 7.0). a) Addition of avidin (1 μM); b) washing with buffer; c) addition of $(NH_4)_2S_2O_8$ (1 mM); d) washing with buffer; e) addition of biotin–$Ni^{II}$cyclam (100 μM); f) buffer wash; and g) addition of $(NH_4)_2S_2O_8$ (1 mM). B) Interferometric reflectance spectra from biotin-functionalized porous silicon. Before addition of avidin (——); after 20 min incubation with avidin (1 μM; ——); and after incubation with biotin–$Ni^{II}$cyclam (100 μM) and $(NH_4)_2S_2O_8$ (1 mM; ——).

idant, the formation of cracks and channels is clear (Figure 4C). The pore size increased to 200–400 nm, which is indicative of a breakdown of the pore structure due to $Ni^{II}$cyclam-induced corrosion. Conversely, upon incubation of avidin presaturated with biotin, followed by addition of biotin–$Ni^{II}$cyclam and oxidant, such effects (EOT slope change, pore size increase) were not observed. Finally, addition of biotin–$Ni^{II}$cyclam (100 μM) and oxidant (1 mM) to an avidin-free porous silicon surface did not induce an EOT slope change.

## Conclusions

We have identified transition metal catalysts, including the aza-crown transition metal complex $Ni^{II}$cyclam, that are capable of corroding porous silicon films by oxidative hydrolysis. Furthermore, we have tethered this complex to bioanalyte species to fashion a transducer of DNA and protein binding. Binding of the analyte–catalyst conjugate leads to an increased effective concentration of the catalyst in the porous silicon layer, transducing the onset of corrosion of the surface into a strong interferometric signal. The signal strength is limited by the turnover rate of the catalyst and by the removal of catalytically active site on the surface due to corrosion. Future efforts will be directed towards optimization of the analytical performance of this sensor platform and further elucidation of the mechanistic aspects of the corrosion process.

This novel transduction concept, involving the conversion of a given biomolecular ligand–receptor recognition into a change in optical thickness of a porous sensor matrix, highlights the potential of such porous silicon transducers for use in biosensor applications. Our approach is compatible with an array format, requires only inexpensive device components such a CCD spectrometer and a white light source, and is conducive to miniaturization. It could find eventually practical utility in biomedical diagnostics, perhaps most appropriately as a transducer for disposable biosensors in point-of-care applications.

## Experimental Section

**Porous silicon etching**: Silicon wafers ($p^{++}$-type, resistivity: 0.6–1.5 mΩcm) were anodized in the dark at 250 mA$cm^{-2}$. Total current was 2.8 C$cm^{-2}$. The thickness of the porous layer was in the range of 3 μm, as determined by scanning electron microscopy images of a cross section of an etched wafer. After etching, the samples were rinsed thoroughly with methanol, acetone, and methylene chloride, and were then carefully dried under a stream of nitrogen.

**Screening of transition metal complexes**: Salen and cyclam complexes were prepared by published procedures.[46,61–64] In brief, equimolar concentrations of ligand and metal salt (either as acetate or chloride) were dissolved in dry methanol or acetonitrile. After having been heated at 60 °C for 4 h, the reaction mixture was allowed to cool to room temperature, and the formed crystals were filtered off and washed with methanol or acetonitrile and then hexane. Bis(hydroxy)salen (salphen) ligands were prepared by condensation of salicylaldehyde derivatives with ethylenediamine or phenylenediamine, respectively.

Interferometric reflectance spectra of porous silicon were recorded with an Ocean Optics spectrometer S 1000 fitted with a bifurcated fiber optic probe. A tungsten light source was focused onto the center of a porous silicon piece with a spot size of approximately 1–2 mm. Spectra were recorded with a CCD-detector in the wavelength range between 400 and 1400 nm. Both the illumination of the surface and the detection of the reflected light were performed along an axis coincident with the surface normal. The effective optical thickness was obtained through Fast Fourier Transformation (FFT) of the spectra. Porous silicon samples were fixated in a custom-made plexiglass flow cell. Solutions of salen and cyclam complexes (1 mM) in PBS (pH 7.0, 100 mM) were prepared and injected into the flow cell by syringe. Ammonium persulfate (1 mM) served as oxidant, while dithiothreitol (1 mM) was used as reductant.

**Characterization of $Ni^{II}$cyclam**: Electrospray mass spectrometry was done on a Series 1100 MSD single quadrupole mass spectrometer (Hewlett Packard). UV/Vis measurements were done on a CARY 100 Bio UV/Vis spectrophotometer from Varian. A 500 MHz Bruker magnet was used for NMR studies.

  

**Cyclam ligand derivatization**: A modification of the Richman–Atkins methodology was used to synthesize the carboxy-derivatized cyclam shown in Scheme 2. We started with the commercially available D,L-2,3-diaminopropionic acid. Tosylation of both amino groups, cesium carbonate promoted cyclization, and subsequent sulfonamide group hydrolysis were carried out as described in the literature. Some selected spectral data for the final compound are as follows: $^1$H NMR (400 MHz, $D_2O$): $\delta = 2.23$ (m, 2H), 2.31 (m, 2H), 3.25 (m, 8H), 3.50 (s, 4H), 3.52 (br s, 2H), 3.54 ppm (t, $J = 6.4$ Hz, 1H); ESI-MS: $m/z$: 267 $[M+Na]^+$.

**Porous silicon functionalizations**: The predominantly hydride-terminated porous layer was exposed to ozone from a Fischer ozone generator with a flow rate of 7.7 g h $^{-1}$ for 10 min. The oxidized samples were vigorously rinsed with methylene chloride, acetone, and methanol, and were then carefully dried under a stream of nitrogen.

**Synthesis of [3-(2-bromoacetamido)propyl]dimethylmethoxysilane**: Bromoacetic acid (1.00 g, 7.2 mmol) was dissolved in methylene chloride (50 mL). 1-[3-(Dimethylamino)propyl]-3-ethylcarbodiimide hydrochloride (EDC, 0.69 g, 3.6 mmol) was added, and the solution was stirred for 30 min, after which (3-aminopropyl)dimethylmethoxysilane (0.93 mL, 6.5 mmol) was injected slowly by syringe. The reaction mixture was stirred overnight. The methylene chloride phase was washed several times with saturated aqueous $NaHCO_3$, dried over $Na_2CO_3$, and evaporated. The crude product was purified by silica chromatography.

**Synthesis of (2-pyridyldithiopropionamidopropyl)-dimethyl-methoxysilane**: Bipyridyl disulfide (3.75 g, 17 mmol) was dissolved in ethanol (99.5%, 20 mL) and glacial acetic acid (0.5 mL). With vigorous stirring, 3-mercaptopropionic acid (0.9 g) in ethanol (5 mL) was added slowly. The reaction mixture was stirred for 12 h at room temperature. After removal of the solvent, the product was purified by neutral alumina column chromatography and dried under high vacuum. The thus prepared 2-pyridyl 3-propionic acid disulfide (0.77 g, 3.6 mmol) was dissolved in methylene chloride (100 mL), and EDC (0.67 g, 3.5 mmol) was added. The mixture was stirred under argon for 30 min, after which (3-aminopropyl)dimethylmethoxysilane (0.5 mL, 3.5 mmol) was injected by syringe. After overnight stirring, the organic phase was washed several times with saturated aqueous $NaHCO_3$, dried over $Na_2CO_3$, and concentrated. The crude product was purified by silica chromatography.

The oxidized porous silicon samples were functionalized by immersing them in a solution (100 mM) of either (2-pyridyldithio-propionamidopropyl)dimethylmonomethoxysilane or [3-(2-bromoacetamido)propyl]dimethylmonomethoxysilane in toluene and heating them at reflux for 3 h. Afterwards, the chips were extensively rinsed in toluene, methanol, acetone, and methylene chloride and dried under a stream of nitrogen. Reduction of the disulfide in a dithiothreitol solution (10 mM) released pyridine-2-thione, which could be quantified by its UV absorption at 343 nm ($\varepsilon = 8080\ M^{-1}\,cm^{-1}$).

Immobilization of thiophosphate DNA (25 μM) on bromoacetamido-functionalized silicon proceeded in DMSO for 2 h (see below). Porous silicon functionalized with (2-pyridyldithiopropionamidopropyl)dimethylmethoxysilane was treated with a DTT solution (10 mM) for 1 h and washed extensively with deionized, distilled water (dd$H_2O$). Subsequently, the reduced surface was submerged in a solution of biotin–HPDP (400 μM, Pierce) for 30 min. The biotinylated surfaces were washed extensively with dd$H_2O$.

**Surface analysis**: FTIR spectra were acquired with a Nicolet Model 550 Magna Series II FTIR instrument in diffused reflectance mode (Spectra-Tech diffuse reflectance attachment). Diffuse reflectance absorption spectra are reported in Kubelka–Munk units. Atomic force microscopy (AFM) images were obtained under ambient conditions with a Nanoscope IIIa Multimode scanning probe microscope (Veeco) operating in Tapping mode. Olympus Nano-Probe tips (OTESPA, Veeco) were used as purchased.

Quantification of DNA immobilization was achieved 1) by comparing the optical density of the incubation solution at 260 nm before and after immobilization, 2) by UV spectroscopic evaluation of pyridine-2-thione released from 3′-dithiopyridyl-5′-thiophosphate DNA upon reduction with DTT (10 mM) for 1 h, and 3) by monitoring of the fluorescence decay of a 3′-fluorescein-labeled 5′-thiophosphate DNA solution in DMSO/100 mM PBS (9:1) upon contact with a porous silicon chip (0.64 $cm^2$) placed at the bottom of a regular fluorescence cuvette.

DNA thermal denaturation profiles were obtained on a thermostated CARY 100 Bio UV/Vis spectrophotometer from Varian at 1 μM duplex concentration in PBS (100 mM, pH 7.0).

**Synthesis of DNA probes**: For hybridization experiments, two orthogonal 5′- or 3′-thiophosphate-terminated DNA oligonucleotides (DNA1 sequence: 5′-pCC GGA CAG AAG CAG AA, DNA2 sequence: 5′-pGC CAG AAC CCA GTA GT-3′) and their corresponding complementary strands (DNA1 and DNA2) were chosen to avoid hairpin loop formation or self-dimerization.

All oligonucleotides were synthesized on an Applied Biosystems 391 DNA synthesizer. 5′-Fluorescein and 5′-thiol modifier (C6) were introduced as 5′-phosphoramidites (Glen Research). 3′-Fluorescein DNA was synthesized from 3′-fluorescein CPG (Glen Research), 5′- thiophosphate DNA by coupling of chemical phosphorylation reagent (Glen Research) to the 5′ end and subsequent oxidation with sulfurizing reagent (Glen Research). 3′-Thiophosphate DNA was prepared with 3′-phosphate CPG and oxidation with sulfurizing reagent after coupling of the first phosphoramidite. Oligonucleotides were deprotected and removed from the CPG with concentrated ammonium hydroxide at 55 °C for 12 h. Oligonucleotides were purified by denaturing polyacrylamide gel electrophoresis (15%) and extracted from the gel by the crush and soak method. Desalting was done with SepPak cartridges (Waters).

Oligonucleotides for attachment to the derivatized cyclam were synthesized with ultraMILD deprotection bases from Glen Research. 5′-Amino modifier (C6) was purchased from Glen Research. Shortly before the conjugation to 5′-amino DNA was performed, the derivatized $Ni^{II}$cyclam complex was prepared as follows: the carboxyderivatized cyclam (30 mg, 0.05 mmol), as its hydrobromide salt, was suspended in DMF (700 μL) and heated to 70 °C. Then, a solution of $NiCl_2$ (400 μM) in DMF (700 μL) was added, and the mixture was heated at the same temperature for 1 h. The formation of the $Ni^{II}$cyclam complex was monitored by the change in the UV absorbance at 450 nm. Conjugation to DNA was done on the CPG in DMF with HBTU and DIEA as base. $Ni^{II}$cyclam-labeled DNA was deprotected with $K_2CO_3$ in methanol (0.05 M) over 4 h at room temperature and purified by size exclusion chromatography.

Oligonucleotides and their fluorescein- or $Ni^{II}$cyclam-labeled derivatives were characterized by mass spectrometry either with a Voyager-DE MALDI-TOF-MS from Applied Biosystems or with a Series 1100 electrospray MS from Hewlett Packard. $Ni^{II}$cyclam-labeled DNA was stored in dd$H_2O$ at 100–1000 μM at −80 °C. All other oligonucleotides were stored at −20 °C.

  

**Synthesis of a biotin–cyclam conjugate**: The carboxy-derivatized cyclam (30 mg, 0.05 mmol), as its hydrobromide salt, was suspended in DMF (700 μL) and heated to 70 °C. A solution of $NiCl_2$ in DMF (400 μM, 300 μL) was added, and the mixture was maintained at 70 °C for 1 h. The formation of the Ni-cyclam complex was monitored by the change in the UV absorbance at 450 nm. After 1 h, the mixture was allowed to cool to room temperature, and the precipitate was collected and washed with DMF to eliminate excess of Ni salt. After the solid had been resuspended in DMF (1.5 mL), HATU (17.5 mg) and DIEA (7.7 μL) were added, which led to the rapid dissolution of the metal complexes. After 20 min of carboxylate preactivation, biotin cadaverine (16.4 mg, Pierce) was added, and the reaction was mixed by sonication for 30 min. A white solid appeared and was removed by centrifugation. The supernatant was evaporated to dryness, yielding a pale green solid, which was thoroughly washed with methylene chloride and methanol. The resulting compound was characterized by mass spectrometry.

**Detection of DNA and avidin**: Binding experiments were carried out in the flow cell described above. Solutions of DNA-$Ni^{II}$cyclam, avidin (Sigma), and biotin–$Ni^{II}$cyclam were prepared in PBS (100 mM, pH 7.0) and injected into the flow cell by syringe. Ammonium persulfate was added at 1 mM concentration. As a control, avidin (1 μM) was preincubated with biotin (100 μM, Aldrich) for 10 min at room temperature.

## Acknowledgements

*This work was generously supported by the US Office of Naval Research (Grants N00014981073 and N000149511293 to MRG). N.H.V. thanks the Deutsche Forschungsgemeinschaft and the Australian Research Council. I.A. thanks the Ministerio de Educacion y Ciencia for postdoctoral fellowships.*

**Keywords:** biosensors · interferometric reflectance · ligand–receptor interactions · optical transducers · oxidation catalysts · porous silicon

[1] F. Xu, G. Zhen, F. Yu, E. Kuennemann, M. Textor, W. Knoll, *J. Am. Chem. Soc.* **2005**, *127*, 13084.
[2] H. Wang, C. X. Zhang, Y. Li, H. L. Qi, *Anal. Chim. Acta* **2006**, *575*, 205.
[3] J. Wang, *Small* **2005**, *1*, 1036.
[4] R. Ince, R. Narayanaswamy, *Anal. Chim. Acta* **2006**, *569*, 1.
[5] F. Scheller, U. Wollenberger, A. Warsinke, F. Lisdat, *Curr. Opin. Biotechnol.* **2001**, *12*, 35.
[6] L. Zhu, E. V. Ansly, *Angew. Chem.* **2006**, *118*, 1208; *Angew. Chem. Int. Ed.* **2006**, *45*, 1190.
[7] F. Lucarelli, G. Marrazza, M. Mascini, *Biosens. Bioelectron.* **2005**, *20*, 2001.
[8] J. Yakovleva, R. Davidsson, M. Bengtsson, T. Laurell, J. Emneus, *Biosens. Bioelectron.* **2003**, *19*, 21.
[9] A. Saghatelian, K. Guckian, D. Thayer, M. Ghadiri, *J. Am. Chem. Soc.* **2003**, *125*, 344.
[10] Y. L. Su, J. R. Li, L. Jiang, J. Cao, *J. Colloid Interface Sci.* **2005**, *284*, 114.
[11] H. Peng, C. Soeller, M. B. Cannell, G. A. Bowmaker, R. P. Cooney, J. Travas-Sejdic, *Biosens. Bioelectron.* **2006**, *21*, 1727.
[12] K. Kerman, Y. Morita, Y. Takamura, M. Ozsoz, E. Tamiya, *Anal. Chim. Acta* **2004**, *510*, 169.
[13] M. Zayats, R. Baron, I. Popov, I. Willner, *Nano. Lett.* **2005**, *5*, 21.
[14] L. T. Canham, *Appl. Phys. Lett.* **1990**, *57*, 1046.
[15] W. Theiss, *Surf. Sci. Rep.* **1997**, *29*, 91.
[16] V. S. Y. Lin, K. Motesharei, K.-P. S. Dancil, M. J. Sailor, M. R. Ghadiri, *Science* **1997**, *278*, 840.
[17] V. M. Starodub, *NATO Sci. Ser. 2* **2002**, *57*, 383.
[18] M. M. Orosco, C. Pacholski, G. M. Miskelly, M. J. Sailor, *Adv. Mater.* **2006**, *18*, 1393.
[19] L. De Stefano, L. Rotiroti, I. Rendina, L. Moretti, V. Scognamiglio, M. Rossi, S. D'Auria, *Biosens. Bioelectron.* **2006**, *21*, 1664.
[20] S. E. Létant, B. R. Hart, S. R. Kane, M. Z. Hadi, S. J. Shields, J. G. Reynolds, *Adv. Mater.* **2004**, *16*, 689.
[21] M. P. Schwartz, A. M. Derfus, S. D. Alvarez, S. N. Bhatia, M. J. Sailor, *Langmuir* **2006**, *22*, 7084.
[22] R. R. K. Reddy, A. Chadha, E. Bhattacharya, *Biosens. Bioelectron.* **2001**, *16*, 313.
[23] S. Chan, S. R. Horner, P. M. Fauchet, B. L. Miller, *J. Am. Chem. Soc.* **2001**, *123*, 11797.
[24] M. J. Schöning, A. Kurowski, M. Thust, P. Kordos, J. W. Schultze, H. Lüth, *Sens. Actuators B* **2000**, *64*, 59.
[25] L. Tay, N. L. Rowell, D. J. Lockwood, R. Boukherroub, *J. Vac. Sci. Technol. A* **2006**, *24*, 747.
[26] S. B. T. de-Leon, R. Oren, M. E. Spira, N. Korbakov, S. Yitzchaik, A. Sa'ar, *Phys. Status Solidi A* **2005**, *202*, 1456.
[27] C. Pacholski, M. Sartor, M. J. Sailor, F. Cunin, G. M. Miskelly, *J. Am. Chem. Soc.* **2005**, *127*, 11636.
[28] L. De Stefano, L. Rotiroti, I. Rea, L. Moretti, G. Di Francia, E. Massera, A. Lamberti, P. Arcari, C. Sanges, I. Rendina, *J. Opt. A* **2006**, *8*, S540.
[29] A. Tinsley-Bown, R. G. Smith, S. Hayward, M. H. Anderson, L. Koker, A. Green, R. Torrens, A. S. Wilkinson, E. A. Perkins, D. J. Squirrell, S. Nicklin, A. Hutchinson, A. J. Simons, T. I. Cox, *Phys. Status Solidi A* **2005**, *202*, 1347.
[30] A. Janshoff, K.-P. S. Dancil, C. Steinem, D. P. Greiner, V. S. Y. Lin, C. Gurtner, K. Motesharei, M. J. Sailor, M. R. Ghadiri, *J. Am. Chem. Soc.* **1998**, *120*, 12108.
[31] K.-P. S. Dancil, D. P. Greiner, M. J. Sailor, *J. Am. Chem. Soc.* **1999**, *121*, 7925.
[32] C. Xiao, R. Boukherroub, J. T. C. Wojtyk, D. D. M. Wayner, J. H. T. Luong, *Langmuir* **2002**, *18*, 4165.
[33] A. M. Tinsley-Bown, L. T. Canham, M. Hollings, M. H. Anderson, C. L. Reeves, T. I. Cox, S. Nicklin, D. J. Squirrell, E. Perkins, A. Hutchinson, M. J. Sailor, A. Wun, *Phys. Status Solidi A* **2000**, *182*, 547.
[34] S. Chan, P. M. Fauchet, Y. Li, L. J. Rothberg, B. L. Miller, *Phys. Status Solidi A* **2000**, *182*, 541.
[35] H. Ouyang, M. Christophersen, R. Viard, B. L. Miller, P. M. Fauchet, *Adv. Funct. Mater.* **2005**, *15*, 1851.
[36] C. Steinem, A. Janshoff, V. S.-Y. Lin, N. H. Voelcker, M. R. Ghadiri, *Tetrahedron* **2004**, *60*, 11259.
[37] E. Engvall, P. Perlman, *Immunochemistry* **1971**, *8*, 871.
[38] W. Nam, H. J. Kim, S. H. Kim, R. Ho, J. S. Valentine, *Inorg. Chem.* **1996**, *35*, 1045.
[39] R. W. Hay, J. A. Crayston, T. J. Cromie, P. Lightfoot, D. C. L. DeAlwis, *Polyhedron* **1997**, *16*, 3557.
[40] L. Canali, D. C. Sherrington, *Chem. Soc. Rev.* **1999**, *28*, 85.
[41] P. Brandt, P.-O. Norrby, A. M. Daly, D. G. Gilheany, *Chem. Eur. J.* **2002**, *8*, 4299.
[42] J. A. Miranda, C. J. Wade, R. D. Little, *J. Org. Chem.* **2005**, *70*, 8017.
[43] B.-B. Jang, K.-P. Lee, J. Suh, *J. Am. Chem. Soc.* **1998**, *120*, 12008.
[44] J. Suh, *Acc. Chem. Res.* **2003**, *36*, 562.
[45] P. W. C. G. Riordan, *J. Am. Chem. Soc.* **1994**, *116*, 2189.
[46] S. S. Mandal, U. Varshney, S. Bhattacharya, *Bioconjugate Chem.* **1997**, *8*, 798.
[47] C. J. Burrows, J. G. Muller, *Chem. Rev.* **1998**, *98*, 1109.
[48] J. F. Kinneary, T. M. Roy, J. S. Albert, H. Yoon, T. R. Wagler, L. Shen, C. J. Burrows, *J. Inclusion Phenom. Mol. Recognit. Chem.* **1989**, *7*, 155.
[49] D. J. Gravert, J. H. Griffin, *Inorg. Chem.* **1996**, *35*, 4837.
[50] J. Suh, W. J. Kwon, *Bioorg. Chem.* **1998**, *26*, 103.
[51] M. Costas, M. P. Mehn, M. P. Jensen, L. Que, Jr., *Chem. Rev.* **2004**, *104*, 939.
[52] D. E. Linn, M. J. Dragan, D. E. Miller, *Inorg. Chem.* **1990**, *29*, 4356.
[53] A. McAuley, C. Xu, *Inorg. Chem.* **1992**, *31*, 5549.
[54] H. R. Pezza, N. Coichev, *J. Coord. Chem.* **1999**, *47*, 107.
[55] J. N. Stuart, A. L. Goerges, J. M. Zaleski, *Inorg. Chem.* **2000**, *39*, 5976.
[56] G. P. Anipsitakis, D. D. Dionysiou, *Environ. Sci. Technol.* **2004**, *38*, 3705.
[57] G. J. Bridger, R. T. Skerlj, S. Padmanabhan, D. Thornton, *J. Org. Chem.* **1996**, *61*, 1519.

  

[58] F. Cesare Marincola, M. Casu, G. Saba, C. Manetti, A. Lai, *Phys. Chem. Chem. Phys.* **2000**, *2*, 2425.
[59] J. Duguid, V. A. Bloomfield, J. Benevides, G. J. Thomas, *Biophys. J.* **1993**, *65*, 1916.
[60] T. Gao, J. Gao, M. Sailor, *Langmuir* **2002**, *18*, 9953.
[61] P. K. Chan, C.-K. Poon, *J. Chem. Soc. Dalton Trans.* **1975**, *5*, 858.
[62] E. G. Samsel, K. Srinivasan, J. K. Koch, *J. Am. Chem. Soc.* **1985**, *107*, 7606.
[63] L. Mao, K. Yamamoto, W. Zhou, L. Jin, *Electroanalysis* **2000**, *12*, 72.
[64] S. Zolezzi, A. Decinti, E. Spodine, *Polyhedron* **1999**, *18*, 897.

Received: February 23, 2008
Published online on June 24, 2008

  